Dynamic range requirements in digital mammography

Andrew D. A. Maidment, Rebecca Fahrig, and Martin J. Yaffe

Dynamic range requirements in digital mammography

Andrew D. A. Maidment,[a] Rebecca Fahrig, and Martin J. Yaffe
Departments of Medical Biophysics and Radiology, University of Toronto, and Research Division,
Sunnybrook Health Science Centre, 2075 Bayview Avenue, Toronto, Ontario, M4N 3M5, Canada

The dynamic range and the number of gray levels, Γ_s, required for digital mammography has been evaluated using an energy transport model. The effects of molybdenum (Mo) and tungsten (W) target spectra and the energy-dependent attenuation by elemental filters, breast tissue, and a phosphor screen were included in the model. For detectors with ideal optical coupling and no inherent detector noise, 3100 gray levels are discernable (requiring 12 bits per pixel), assuming a 40 kVp, W target spectrum (1.0 mm Al filtration), a mean glandular dose to a 5 cm thick breast of 0.6 mGy, and an ideal observer with a 5 mm diam viewing aperture. The effects of inherent detector noise and realistic coupling efficiencies on Γ_s were also examined. For the 40 kVp, W spectrum, a detector with total coupling efficiency of 16 electrons (e^-) per x-ray interaction and a dynamic range of 3000 (maximum carrier signal of 1.93×10^5 e^-/pixel and inherent detector noise of 64 e^- pixel) would decrease the number of gray levels that could be resolved by only 2% compared to a detector with ideal coupling and no inherent noise. A detector with a total coupling efficiency of 2.0 electrons per x-ray interaction and a dynamic range of 240 (maximum carrier signal 2.41×10^4 e^-/pixel and inherent detector noise of 100 e^-/pixel) would reduce the number of gray levels by 26% for the 40 kVp spectrum. On the basis of dynamic range, W spectra are preferable for digital mammography, since Mo spectra yielding the same signal-to-noise ratio require a detector with dynamic range twice as large, and with a 30% greater saturation signal. When no scatter rejection method is used, scattered radiation over a 254 cm^2 imaging field reduces the number of discernable gray levels by 23% for a 5 cm thick breast and 34% for an 8 cm thick breast.

Key words: digital mammography, dynamic range, dose, signal-to-noise ratio, detector design

I. INTRODUCTION

Film-screen mammography is currently the most sensitive imaging modality available for the early detection of breast cancer.[1-3] Nevertheless, the detection of subtle lesions using film-screen mammography can be limited by film-screen technology.[4] Because the range of exposures exiting the compressed female breast exceeds the range over which the display contrast gradient of film-screen combinations is near maximum,[4,5] highly attenuating and highly transmissive regions of the breast are often imaged with suboptimal contrast. In these regions, film granularity noise is nearly equal to x-ray quantum noise at zero spatial frequency,[6] while at high spatial frequencies, film granularity noise can exceed x-ray quantum noise.[6,7] Radiation scattered by the breast and incident upon the image receptor reduces contrast,[8] and current scatter rejection methods necessitate a two- to threefold increase in dose.[9] Digital mammography has the potential to overcome these limitations.[4,10] In this paper, the signal handling requirements of an x-ray detector for digital mammography are considered.

Figure 1 illustrates a digital mammography detector of the type currently under development at the University of Toronto.[11,12] The detector consists of an x-ray scintillating phosphor coupled optically to a charge-coupled device (CCD) image array. X rays absorbed in the phosphor produce light quanta, which are then converted by the image array into electrons. The digitized electronic signal forms the image. In Fig. 2, a simplified schematic illustrates the

signals obtained with a detector for a uniformly attenuating breast containing a small uniform lesion. In order to allow reliable detection of subtle structures in the breast, a detector must be able to record a wide range of *carrier signals (Q)* corresponding to the range of radiation intensities transmitted through the breast. The detector must also be able to faithfully record small changes, or *image signals (ΔQ)*, anywhere in the range of carrier signals. As shown by Rose,[13] this implies that ΔQ must exceed the noise or fluctuation in the carrier signal by some safety factor. It is also important that the maximum carrier signal does not exceed the maximum or "saturation" signal (Q_{sat}) of the image array. In CCD image arrays this can cause "blooming" artifacts, in which spatial localization of charge is lost.

Another consideration when designing a digital mammography system is the presence of *quantum sinks.*[14] The phosphor screen is the *primary quantum sink,* as not all x rays are detected by a phosphor screen of finite thickness. Ideally, image noise should be dominated by the random fluctuations in the number of quanta detected at this point. A *secondary quantum sink* occurs if the number of quanta or electrons at a subsequent stage in the imaging system is smaller than the number of x-ray quanta detected. Under such conditions, image noise is dominated by the statistical fluctuations in the number of secondary quanta.[14] All optically coupled systems involve a loss of some light quanta, therefore, the optical coupling must be designed to ensure
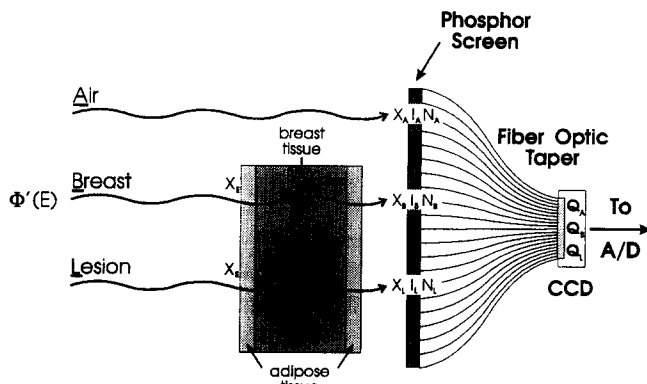
FIG. 1. Cross section of the x-ray detector, the modeled semicylindrical breast, the cylindrical lesion, and the three regions of interest: air (A), breast (B), and breast+lesion (L). X_E is the entrance exposure, and X_A, X_B, and X_L are detector exposures. I and N are the numbers of x-ray quanta incident upon and attenuated by the phosphor, and Q are the corresponding charges in the CCD.

that no information is lost due to secondary quantum sinks and to ensure that the entire range of carrier signals emitted from the phosphor can be recorded by the image array.

In this paper, the method of Motz and Danos[15] is extended to model x-ray detectors for digital mammography, and a method is presented to calculate the dynamic range and number of gray levels required for specific imaging tasks typical of digital mammography. An energy transport model of the propagation of signal and noise is used to calculate breast entrance exposure, mean glandular dose, detector exposure, and the light quanta fluence from a phosphor screen for a given detector exposure. Assuming a mean glandular dose to the breast similar to that of film-screen mammography, the expected maximum detector exposure is calculated, and the required maximum signal handling capability of the image array is obtained. The minimum detectable image signal is also calculated. This signal determines the maximum allowable inherent detec-

FIG. 2. Schematic illustrating carrier signals (Q) and the image signal (ΔQ). The breast, lesion, and air regions correspond to those shown in Fig. 1.

tor noise for a given imaging task. The required dynamic range of the detector, the number of gray levels, and the required number of bits per pixel are then determined. The dynamic range and related parameters are calculated for molybdenum (Mo) and tungsten (W) target x-ray sources over a range of kilovoltages for different breast and lesion compositions and thicknesses. The effect of scattered radiation is also considered. This method can be used to guide the design and the selection of imaging components, to predict the number of quanta at any point in the image detector, to determine the presence of secondary quantum sinks, and to make accurate estimates of detective quantum efficiency.

II. THEORY

A. Production of a digital image

The interactions of the x-ray beam are examined in three regions, shown in Figs. 1 and 2, which correspond to a path (A) through air just beside the breast; a path (B) through normal breast tissue only; and a path (L), which passes through both normal breast tissue and a tissue-replacing lesion. The breast is modeled as a semicylinder with a superficial layer of adipose tissue surrounding a homogeneous mixture of specified ratios of adipose and fibroglandular tissue. The entrance exposure to the breast is X_E and the mean glandular dose to the breast is D_g. X_A, X_B, and X_L are the exposures to the screen for the three paths. For the parallel beam geometry assumed in this paper, X_A is equal to X_E. A complete list of symbols is provided in Table I.

The CCD image array has photosensitive picture elements (pixels) of area a_I, which because of demagnification in the detector, correspond to an area at the surface of the x-ray absorbing phosphor of a_P. The total number of x-ray quanta incident upon the screen per unit area is given by $I=I'+I''$, and the total number interacting in the screen per unit area is $N=N'+N''$. The prime ($'$) and double prime ($''$) denote primary and scattered x-ray quanta. The carrier signal, Q, is given by the total number of electrons generated per pixel, i.e., $Q=Q'+Q''$. I, N, and Q are given subscripts A, B, or L corresponding to "air," "breast," and "lesion" data, respectively.

The number of electrons collected in one pixel of the CCD image array due to the interaction of primary quanta, Q', is

$$Q'=a_P C_D \int_0^{E_{max}} \frac{d\Phi'(E)}{dE} T(E)\eta'(E)\bar{g}(E)dE. \quad (1)$$

The optical coupling efficiency, C_D, is equal to the mean probability that a light quantum emitted from the phosphor screen will generate an electron–hole pair in the CCD. C_D is given by the product of the quantum efficiency of the CCD image array to light[16] and the coupling efficiency of the intervening optics. The peak x-ray energy is E_{max}, $d\Phi'(E)/dE$ is the differential primary x-ray photon fluence (expressed at the entrance to the breast) with energy between E and $E+dE$. The narrow beam x-ray transmission for a path through each of the three regions is
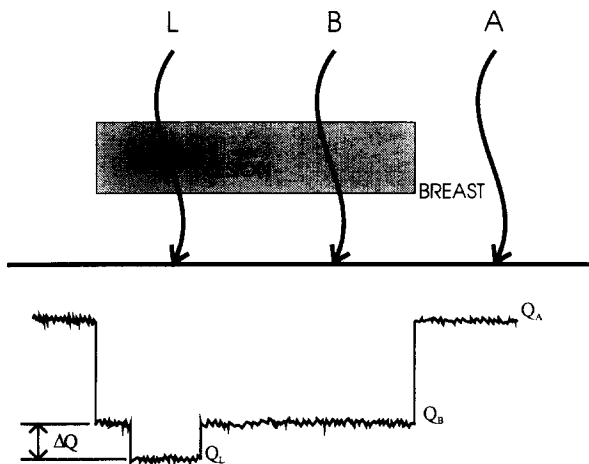
TABLE I. Table of symbols.

Symbol	Description
Γ_C	Carrier signal ratio $(=Q_A/Q_B)$
Γ_D	Image array dynamic range $(=Q_{sat}/\sigma_D)$ [Eq. (12)]
Γ_S	Image signal ratio $(=Q_{max}/k\sigma_{\Delta Q_{min}})$ [Eq. (11)]
$\tilde{\Gamma}_S$	Image signal ratio normalize by $D_g^{-1/2}$ and $a_L^{-1/2}$
Γ_X	Exposure ratio $(=X_A/X_B)$
η'	Quantum detective efficiency of the phosphor screen for primary radiation
η''	Quantum detective efficiency of the phosphor screen for secondary radiation
σ_D	Image array inherent detector noise
σ_Q	Noise in carrier signal (subscripts B and L denote breast and lesion regions)
$\sigma_{\Delta Q}$	Noise in image signal [Eqs. (6) and (7)]
$\Phi'(E)$	The differential primary x-ray photon fluence
a_P, a_I	Pixel area at phosphor screen and at the CCD image array
a_L	Lesion area
A_S	Swank factor of the phosphor screen
C_D	Conversion factor between the signal in the image array and the number of light quanta emitted from the phosphor screen
C_M	Modulation Contrast [Eq. (9)]
D_g	Mean glandular dose to the breast
$\bar{g}(E)$	Average number of light quantum emitted from the phosphor screen for each x ray of energy E, interacting
I, I', I''	Number of x-ray quanta incident upon the screen per unit area (total, primary, and scattering, respectively)
k	Rose's threshold SNR [Eq. (5)]
k'	Number of gray levels that represent the range of charges from Q to $Q+\Delta Q$
N, N', N''	Number of x-ray quanta interacting in the screen per unit area (total, primary, and scattered x-ray quanta, respectively)
Q, Q', Q''	Number of electrons generated in the image array per pixel (in total, and due to primary and secondary x-ray quanta, respectively)
$\tilde{Q}$	Q normalized by D_g and a_L
Q_{sat}	Saturation carrier signal of the image array
ΔQ	Image signal [Eq. (4)]
ΔQ_{min}	Minimum image signal as defined by Rose's criterion [Eq. (5)]
$T(E)$	Transmission of primary quanta through each region (air, breast, and lesion)
X_E	Entrance exposure to the breast
X_A, X_B, X_L	Detector exposure in the air, breast, and lesion regions

given by $T(E)$. $\eta'(E)$ is the primary x-ray quantum detection efficiency (QDE) of the phosphor screen, and $\bar{g}(E)$ is the mean conversion gain of the screen (number of light quanta emitted per interacting x ray) for x-ray quanta, that interact with incident energy E. The integral (of the x-ray spectrum) number of primary x-ray quanta incident upon the screen and the number interacting with it may be calculated in a manner similar to Eq. (1) as I and N, respectively. Integration over the incident spectrum may also be used to calculate the average value, η, of the QDE and the spectrum-averaged conversion gain of the phosphor screen, $\bar{g}$. The total coupling efficiency, $\bar{g}C_D$, gives the average number of electrons produced in the CCD image array per x-ray interaction.

At mammographic energies, the presence of scattered radiation does not significantly shift the spectral energy

distribution of the x-ray beam.[17] Scattered x-ray quanta do, however, have a higher probability of interaction than primary x-ray quanta of similar energy because of increased path length in the phosphor.[18] The number of electrons collected per pixel due to the interaction of scattered radiation, Q'', is

$$Q'' = a_P C_D \frac{I''}{I'} \int_0^{E_{max}} \frac{d\Phi'(E)}{dE} T(E)\eta''(E)\bar{g}(E)dE, \quad (2)$$

where $\eta''(E)$ is the phosphor interaction efficiency of scattered radiation. The work of Dance and Day[19] was used to estimate the increased interaction efficiency of scattered radiation, $\eta''(E)/\eta'(E)$, in the phosphor screen. Dance and Day have shown that the variation of the ratio of interaction efficiencies with breast thickness is small. The ratio of scattered to primary x-ray quanta (SPR) incident upon the detector is I''/I', which, over the range of energies considered in this paper, may be treated as being independent of photon energy.[19]

The noise (expressed as the standard deviation) in Q, the collected charge per pixel, is given by[20]

$$\sigma_Q = \left[a_P \int_0^{E_{max}} \frac{d\Phi'(E)}{dE} T(E)\left(\eta'(E) + \eta''(E)\frac{I''}{I'}\right) \right.$$

$$\left. \times \left(\frac{\bar{g}^2(E)C_D^2}{A_S(E)} + \bar{g}(E)C_D(1-C_D)\right)dE + \sigma_D^2 \right]^{1/2}, \quad (3)$$

where $A_S(E)$ is the Swank factor or scintillation efficiency[21] of the phosphor and σ_D is the inherent detector noise. This equation is exact below the K edge of gadolinium (50.2 keV), where K x-ray fluorescence is not a factor. This condition applies for the spectra of interest for digital mammography. Optical coupling and charge conversion in the detector are treated as binomial distributions. The inherent detector noise is given by the standard deviation of the signal obtained per pixel without x-ray irradiation, and includes fluctuations in the CCD dark current and charge readout. The symbols σ_A, σ_B, and σ_L are used to represent the fluctuation, σ_Q, calculated in the air, breast, and lesion regions, respectively.

It is assumed that the detection of a lesion is performed by an ideal observer (i.e., one that integrates the signal and noise over a region of interest). Thus the image signal, ΔQ, must be calculated over the entire area of the lesion, as given by

$$\Delta Q = \frac{a_L}{a_P}(Q_B - Q_L), \quad (4)$$

where a_L is the area of the lesion, and a_L/a_P is the number of pixels in the lesion. In this calculation, an area of normal breast tissue equal to that of the lesion is considered. Following Rose,[13] the minimum reliably detectable image signal is given by

$$\Delta Q_{min} = k\sigma_{\Delta Q}. \quad (5)$$

Rose has shown that k typically has a value of 4 or 5. This value is based on the assumption that the structure of the expected image is unknown. It should be noted that k is

not precisely defined, and can vary by a factor of 2 or more. In keeping with the assumption of an ideal observer, the noise in the image signal, $\sigma_{\Delta Q}$, is calculated as the quadrature sum of the pixel-to-pixel noise over the area of the lesion:

$$\sigma_{\Delta Q} = \left(\frac{a_L}{a_P} (\sigma_B^2 + \sigma_L^2) \right)^{1/2}. \tag{6}$$

For low contrast objects, $\sigma_B \approx \sigma_L$, and we obtain

$$\sigma_{\Delta Q} = \sigma_B \sqrt{2a_L/a_P}. \tag{7}$$

To compare detectors for which display contrast may be modified after image acquisition, the signal-to-noise ratio of the lesion (LSNR), defined as

$$\text{LSNR} = \frac{\Delta Q}{\sigma_{\Delta Q}}, \tag{8}$$

is calculated. In such detectors, the limits of detectability are determined by the LSNR. To allow comparison with detectors that lack the ability to alter display contrast (e.g., film-based imaging systems), the modulation contrast, C_M, is calculated using

$$C_M = \frac{Q_B - Q_L}{Q_B + Q_L}. \tag{9}$$

In such detectors, the limits of detectability may be determined by the minimum observable display contrast.

B. Performance measures

The detective quantum efficiency (DQE) describes the transfer of the carrier signal-to-noise ratio (SNR) through the detector, and is given by

$$\text{DQE} = \frac{\text{SNR}_{\text{out}}^2}{\text{SNR}_{\text{in}}^2}. \tag{10}$$

The carrier SNR at the input of the detector is given by the ratio of the incident x-ray quanta per pixel to the noise (which is Poisson distributed), i.e., $\text{SNR}_{\text{in}} = (I a_P)^{1/2}$. The carrier SNR at the output is the ratio of the corresponding carrier signal to the noise in that signal, i.e., $\text{SNR}_{\text{out}} = Q/\sigma_Q$, where Q and σ_Q are given by Eqs. (1)–(3).

As described above, it is necessary that a detector be able to record a wide range of carrier signals. The region surrounding the breast provides the least attenuation, hence the maximum carrier signal $Q_{\text{max}} = Q_A$. For a particular breast thickness and composition, the *carrier signal ratio* is defined as $\Gamma_c = Q_{\text{max}}/Q_B$. The ratio of detector exposures that produces these carrier signals is the *exposure ratio*, Γ_x, given by X_A/X_B. A detector suitable for digital mammography must be able to record a dynamic range of carrier signals greater than Γ_C.

It is even more important that a detector faithfully record sufficiently small image signals, i.e., the imaging system must be able to satisfy Rose's criterion over the entire range of exposures presented to the detector. The *image signal ratio*, Γ_S, is defined as

$$\Gamma_S = \frac{(a_L/a_P)Q_{\text{max}}}{k\sigma_{\Delta Q_{\text{min}}}}, \tag{11}$$

the ratio of the maximum carrier signal to the minimum detectable image signal, as given in Eq. (5). Γ_S describes the number of times the small signal per pixel, $\Delta Q_{\text{min}} a_P/a_L$, fits into the range 0 to Q_{max}, assuming a linear detector. Thus, Γ_S is the number of *reliably discernable gray levels in an image*. The number of *digitization levels* is defined as $k' \Gamma_S$. Motz and Danos[15] have suggested that to extract all the information contained in a signal with Poisson fluctuations, the x-ray quantum fluctuations must be displayed. This would require k' to be greater than unity. In this paper, we assume that $k' = 20$ (i.e., a single gray level increment is equal to one-fourth that of $\sigma_{\Delta Q_{\text{min}}}$). The choice of k' is influenced by the ability to estimate $\sigma_{\Delta Q_{\text{min}}}$, and to minimize the effect of digitization noise. The values of $\sigma_{\Delta Q_{\text{min}}}$ and, hence Γ_S, are dependent upon the maximum lesion area, a_L, compatible with the assumption of the ideal observer. The choice of a_L is described further in Sec. III. A linear detector was considered in this model to simplify the analysis of the propagation of noise, and to allow future evaluation of the spatial-frequency dependence of the propagation of signal and noise.

Γ_S can also be used to prescribe the required dynamic range of the digital mammography detector for a particular detection task. CCD image arrays are specified in terms of the saturation carrier signal or "well capacity," Q_{sat}, and the inherent detector noise, σ_D. The actual dynamic range of the image array, Γ_D, is given by

$$\Gamma_D = Q_{\text{sat}}/\sigma_D. \tag{12}$$

When designing a digital mammography detector, one must ensure that the saturation carrier signal is not exceeded (i.e., $Q_{\text{sat}} \geqslant Q_{\text{max}}$) and that image noise is x-ray quantum limited rather than device limited (i.e., $\sigma_D \ll \sigma_B$). Since the fluctuations in the number of secondary quanta affect the fluctuations in the recorded carrier signals, the coupling factor, C_D, and the average screen conversion gain, $\bar{g}$, should be such that $\bar{g} C_D \gg 1$, to avoid a secondary quantum sink.[14] These requirements can be used for the design specifications of Q_{sat} and Γ_D of a suitable digital mammography detector. In Sec. IV B, the effects of $\bar{g} C_D$ and σ_D on the values of Γ_S and Γ_D are calculated. Values of Γ_D must be chosen so as to minimize the reduction in the value of Γ_S.

III. METHODS AND MATERIALS

X-ray spectra were obtained from both measured and calculated data. Molybdenum target spectra were calculated at 1 kVp intervals, based on the bremsstrahlung model of Tucker *et al.*,[22(a)] with characteristic radiation added according to measured spectra provided by Fewell and Jennings.[22(b)] The W target spectra have been interpolated to 1 kVp intervals from measured spectra.[22(b)] All spectra have an inherent filtration of approximately 1 mm of beryllium. A filtration of 30 μm of Mo, which is typical of that used in film-screen mammography, was added to

the Mo spectra. The W spectra have an additional filtration of 1.0 mm aluminum. We are currently investigating the choice of the optimal beam filtration for Mo and W spectra in digital mammography.[23] Although a parallel beam geometry is assumed in our simplified model, all fluence values stated for the sources used are typical of those that would be measured 60 cm from the focal spot. This geometry allows flexibility in choice of source-skin distance (SSD) and source-image distance (SID) in subsequent calculations. The exposure data are calculated from the x-ray fluence using the method of Johns and Cunningham.[24] For a diverging beam geometry, the entrance exposure, X_E, will increase relative to the detector exposure (X_A, X_B, or X_L) due to the inverse square law, and a simple correction can be made for a specific geometry. As such, the calculated value of the mean glandular dose would increase relative to the parallel beam case.

The breast is modeled based on the assumptions used by Wu et al.[25(a)] for their calculation of an absorbed dose. As a typical case, a 5 cm thick "medium" breast[26] is modeled with two 0.4 cm thick layers of adipose tissue and 4.2 cm of 50% adipose, 50% fibroglandular tissue. As a limiting case, an 8 cm thick breast is modeled with adipose layers and 7.2 cm of 100% fibroglandular tissue. The breast, shown in schematic in Fig. 1, provides a uniform background for a small lesion. The breast has a semicircular projected cross section of radius 12.7 cm, which provides a large-sized scatter field of 254 cm^2 for the dose calculations. While radiation exposure is readily measurable, the glandular tissue dose is of greater significance as an indicator of risk,[27] and in this paper, therefore, we use the mean glandular dose for this purpose. The mean glandular dose, D_g, is calculated using energy-weighted summation over the x-ray spectra of monoenergetic "dose per incident x-ray quantum" data.[25(a),(b)]

Three cylindrical lesions are modeled: a 0.5 mm thick, 5 mm diam infiltrating ductal carcinoma (IDC) lesion; a 5 mm thick, 5 mm diam IDC lesion; and a 0.1 mm thick, 0.2 mm diam microcalcification. Using data obtained with a contrast-detail phantom, it has been shown[4,10] that a 5 mm diam lesion with subject contrast of 0.5% represents the limit of detectability in a screen-film system. That analysis was performed using a 30 kVp Mo spectrum with 30 μm of Mo filtration and a mean glandular dose of 0.6 mGy to a 5 cm thick lucite contrast-detail phantom. The 0.5 mm thick IDC lesion in the 5 cm thick breast has a subject contrast of 0.5% for the same spectrum, representing a detection task of similar difficulty. For a digital mammography system to match the performance of film-screen mammography, this lesion must be detectable using an equal or lower dose. In this paper, a 5 mm lesion area is used to calculate $\Delta Q_{\min}$. The modeled 5 mm thick IDC[1,28,29] and the microcalcification[30–33] represent clinically relevant detection tasks.

Elemental attenuation coefficients were taken from Plechaty et al.[34] Attenuation coefficients for breast adipose tissue, fibroglandular tissue, and IDC were interpolated using measured data from Johns and Yaffe.[35] Calcifications are assumed to have the attenuation properties of calcium
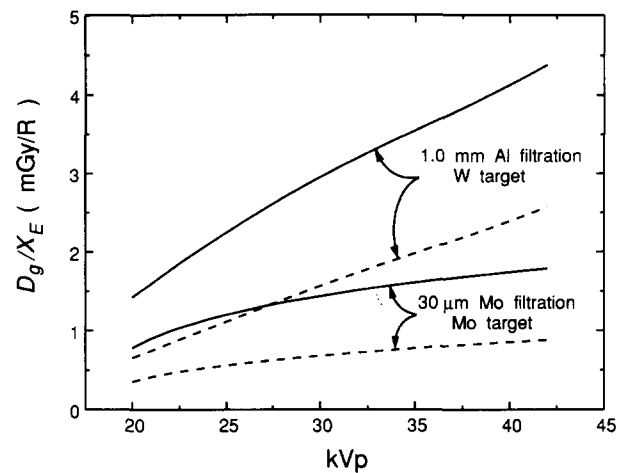

FIG. 3. The relationship between the mean glandular dose (D_g) and the entrance exposure (X_E) for the 5 cm thick 50/50 breast (solid), and the 8 cm thick fibroglandular breast (dashed). These data were calculated from "dose per incident x-ray quantum" data provided by Wu [Ref. 25(b)].

hydroxyapatite[36] [$Ca_5(PO_4)_3OH$] with a density of 3.2 g/cm^3. In this study, a Kodak Min-R (equivalent to the Kodak Lanex Fine) mammographic phosphor screen is used. This screen consists of 31.7 mg/cm^2 $Gd_2O_2S:Tb$ phosphor material.[37] Data on the number of light quanta produced in the screen, $\bar{g}(E)$, the x-ray quantum detection efficiency, $\eta(E)$, and the scintillation efficiency, A_S, were obtained from Trauernicht and Van Metter,[38] and Dick and Motz.[39] These data were experimentally measured as a function of incident energy.

IV. RESULTS AND DISCUSSION

In the following sections we consider (a) an idealized detector, (b) a more realistic detector, and (c) the effect of scattered radiation.

A. Idealized detector

Initially, an idealized detector is considered in which a Kodak Min-R phosphor screen is perfectly coupled ($C_D=1$) to a noiseless image array ($\sigma_D=0$). It is assumed that an ideal grid is placed between the breast and the detector (i.e., $I''=0$).

The mean glandular dose per unit entrance exposure data, D_g/X_E, for the two target materials and two modeled breasts shown in Fig. 3. In Fig. 4, incident Mo and W spectra at 30 kVp are shown as examples. For the 30 kVp Mo spectrum 3.3×10^4 x rays mm^{-2} mR^{-1} are incident, with a mean energy of 16.8 keV. For the 30 kVp W spectrum 5.5×10^4 x rays mm^{-2} mR^{-1} are incident with a mean energy of 21.5 keV. These numbers are in agreement with the work of Barnes and Chakraborty.[40]

Using these data, the charge collected per unit area and mean glandular dose to the breast, $\bar{Q}=Q(a_P D_g)^{-1}$, was calculated for the region surrounding the breast, $\bar{Q}_A$. The normalization by dose and area allow easy comparison of various detectors and lesions. These results are shown in Fig. 5 for the two modeled target materials and two mod-
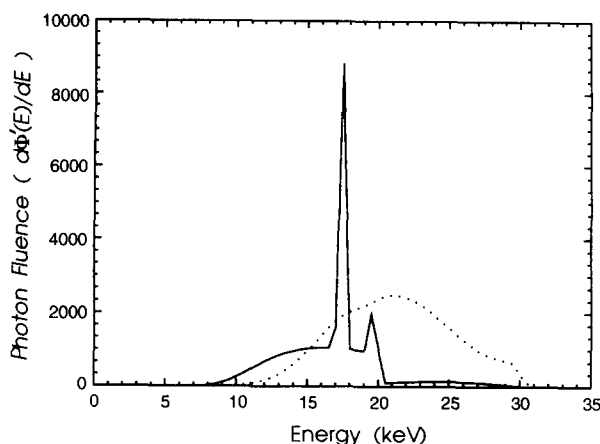
FIG. 4. Incident spectra produced by 30 kVp Mo (solid) and W (dashed) sources.

eled breasts. These carrier signal data are used to calculate Q_{max}, which is the minimum required value for Q_{sat}. Regardless of breast composition and anode material, Q_A decreases with increasing kVp. At any tube potential, the W spectrum yields a value of $\tilde{Q}_A$ that is smaller than that obtained with the Mo spectrum because of the lower mean glandular dose per unit entrance exposure of the Mo spectra. Tungsten spectra also produce values of $\tilde{Q}_A$ that vary less with breast thickness and composition than do Mo spectra. Similarly, $\tilde{Q}_A$ is larger for the 8 cm breast than for the 5 cm breast, because the mean glandular dose per unit entrance exposure (i.e., X_E, and hence X_A) is lower for the 8 cm breast than for the 5 cm breast. Therefore, for a given dose to the breast, use of the W spectra requires a lower value of Q_{sat} than for the Mo spectra.

The effect of applied x-ray tube potential on Γ_C and Γ_X for the W and Mo spectra is shown in Figs. 6(a) and 6(b) for the 5 and 8 cm thick breasts, respectively. At any energy, the W spectrum produces values of Γ_C and Γ_X that
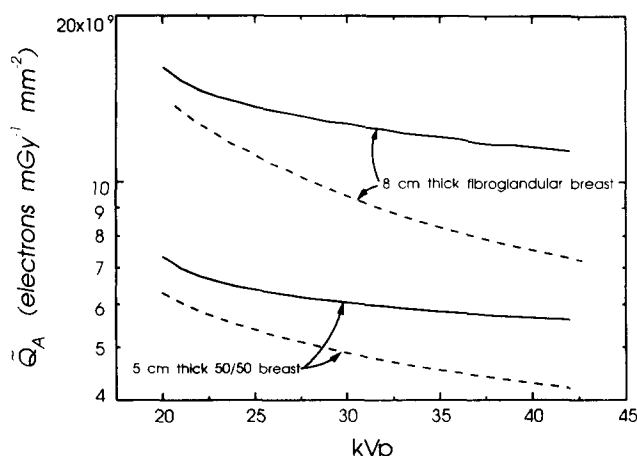

FIG. 5. The maximum carrier signal (electrons) in a narrow region surrounding the breast ($\tilde{Q}_A$) per mm^2 per mGy mean glandular dose to the breast for a detector with perfect coupling ($C_D=1$) shown for a Mo target x-ray tube with 30 μm of Mo filtration (solid) and a W target x-ray tube with 1.0 mm of aluminum filtration (dashed).
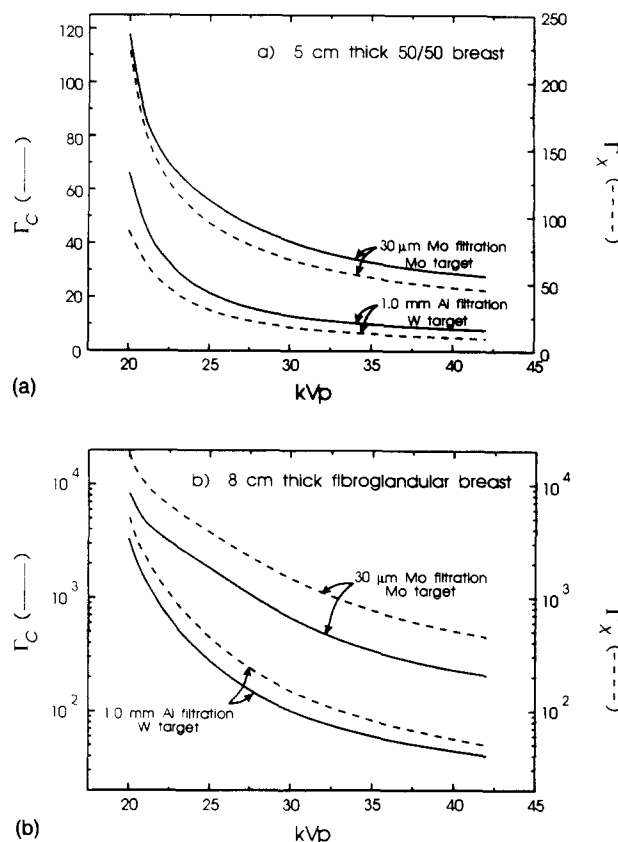

FIG. 6. The carrier signal ratio (solid), and exposure ratio (dashed) of the W and Mo spectra for (a) the 5 cm thick 50/50 breast and (b) the 8 cm thick fibroglandular breast.

are significantly smaller than those obtained with the Mo spectrum. When Γ_C and Γ_X for the 5 cm breast are compared to the 8 cm breast, the values produced by the Mo spectra increase more than the values produced by the W spectra. For example, at 30 kVp, the value of Γ_C for the W spectrum for the 8 cm breast is 7.7 times greater than the value for the 5 cm breast, while the value for the Mo spectrum increases 16.3 times. These results occur because thicker breasts and lower mean energy x-ray beams result in greater attenuation of the x-ray beam, and hence a greater range of carrier signals are produced in the detector. Thus, W spectra require detectors that are sensitive to a smaller range of carrier signals than the Mo spectra for a given kVp. Increases in Γ_X are even greater. For example, we see that for the 30 kVp Mo spectrum Γ_X is 68 for the 5 cm breast and 1470 for the 8 cm breast. For the same spectra, the values of Γ_C are 41 and 660, respectively. These data indicate that exposure ratios do not give a useful idea of detector dynamic range requirements. The differences between values of Γ_C and Γ_X arise mainly from differences in the energy dependence of the x-ray attenuation and absorption coefficients of the phosphor and of air. These differences demonstrate the need to calculate the charge collected in the CCD to accurately determine the range of carrier signals that are generated in the image array.
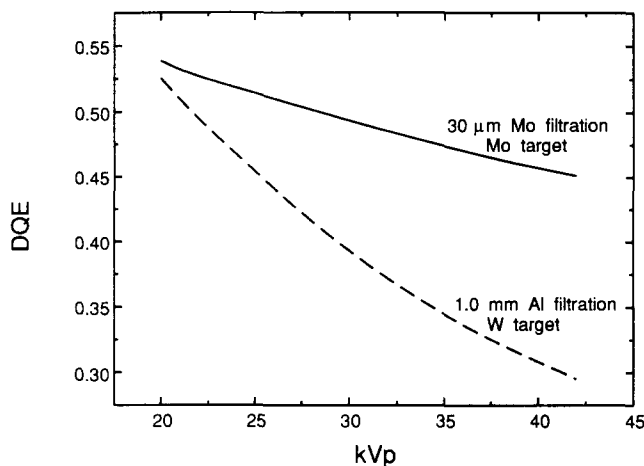
FIG. 7. The DQE of a Min-R screen based detector with perfect coupling and no detector noise. The spectra have been filtered by the 5 cm thick 50/50 breast, and are shown for a Mo target x-ray tube with 30 μm of Mo filtration (solid) and a W target x-ray tube with 1.0 mm of aluminum filtration (dashed).
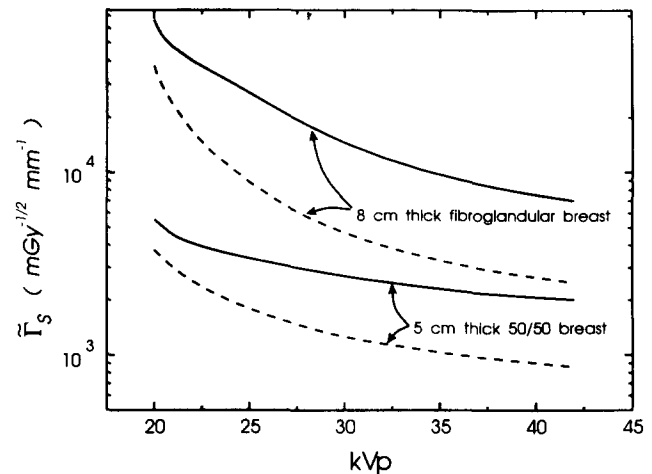
FIG. 8. The image signal ratio per square root area and mean glandular dose, $\tilde{\Gamma}_S$, for the Mo (solid) and W (dashed) spectra. Shown are the data for a Min-R screen based detector with perfect coupling and no inherent detector noise. $\tilde{\Gamma}_S$ is shown for the 5 cm thick 50/50 breast, and the 8 cm thick fibroglandular breast.

It is also necessary to consider the propagation of noise. The relative efficiency of the transfer of signal and of noise from the incident x-ray quanta to the corresponding carrier signals is given by the DQE, shown in Fig. 7. The DQE data were calculated using Eqs. (1), (3), and (10) for W and Mo spectra and include the effect of attenuation by the 5 cm thick breast. Molybdenum spectra yield higher values of DQE than W spectra for the same applied tube voltage because more x-ray quanta are attenuated by the detector (i.e., the QDE is higher) at the lower mean energy of the Mo spectra.[20] DQE values for Mo spectra vary less with applied x-ray tube potential than do those for W spectra, because the Mo characteristic radiation reduces the variation of the mean energy of the spectra.

The DQE, as defined here, relates to the efficiency of SNR propagation of the carrier, while the information required for the detection of a lesion is contained in the image signal, ΔQ, as defined in Eq. (4). The minimum image signal, ΔQ_{min}, is related to Q_{max} by Γ_S. For comparison of various detectors and spectra, Γ_S is normalized by the square root of lesion area and mean glandular dose, i.e, $\tilde{\Gamma}_S = \Gamma_S (a_L D_g)^{-1/2}$. Shown in Fig. 8 is $\tilde{\Gamma}_S$ for the 5 cm thick and 8 cm thick breasts, calculated assuming $k = 5$. $\tilde{\Gamma}_S$ decreases with increasing applied tube potential. At any tube potential, the value of $\tilde{\Gamma}_S$ is greater for the Mo spectrum than for the W spectrum. Above 27 kVp for the 5 cm breast and above 21 kVp for the 8 cm breast, the value of $\tilde{\Gamma}_S$ for Mo spectra is more than twice that for the W spectra. Values for the 8 cm thick breast are more than 3.5 times greater than for the 5 cm thick breast with the Mo spectra and more than 2.9 times greater for the W spectra. The variations in $\tilde{\Gamma}_S$ arise from the energy- and filtration-dependent variations in Q_{max} and ΔQ_{min}. Q_{max} decreases as a function of increased kVp, as described above. However, ΔQ_{min}, which increases as a function of increasing kVp, has a greater effect on $\tilde{\Gamma}_S$. For example, the value of Q_{max} drops by 25% between 20 and 42 kVp for the Mo spec-

trum. On the other hand, the value of ΔQ_{min} doubles over this range, because although the QDE of the phosphor is lower for spectra with higher mean energies, more x rays are incident upon the phosphor for the same dose to the breast, and those x rays that do interact each deposit a greater amount of energy.

As described in Sec. II B, the number of gray levels that may be discerned with a particular spectrum, breast thickness, and composition is proportional to Γ_S. Thus the data presented in Fig. 8 indicate, for example, that more gray levels are discernable with Mo spectra than W spectra. However, if a lesion is detectable with the threshold LSNR [Eq. (8)] and the same mean glandular dose to the breast with two different spectra, then the spectrum that requires the smallest number of gray levels should be used, since detector requirements are less stringent. To evaluate whether both Mo and W spectra can be used to detect lesions with comparable SNR and dose, the image signal normalized per unit area and mean glandular dose, $\Delta \tilde{Q} = \Delta Q (a_L D_g)^{-1}$, was calculated for the three lesions and two target materials described above. $\Delta \tilde{Q}$ is shown for the 5 cm thick breast in Fig. 9(a), and for the 8 cm thick breast in Fig. 9(b). For all lesions, the W spectra produce image signals that are 40%–50% greater than the image signals produced with Mo spectra of the same peak energy and for the same dose to the breast. Although the W spectra have higher mean energy, and hence lower subject contrast, the exit exposure from the breast is greater than with Mo spectra for the same dose to the breast and the same applied voltage, as demonstrated by Fig. 6. Thus a greater number of x-ray quanta are absorbed in the phosphor material, resulting in a greater image signal with W spectra, even though the W spectra produce lower values of DQE for the carrier.

In Figs. 10(a) and 10(b), the modulation contrast of the three lesions is shown when imaged with Mo and W spectra for the 5 and the 8 cm breasts, respectively. In spite
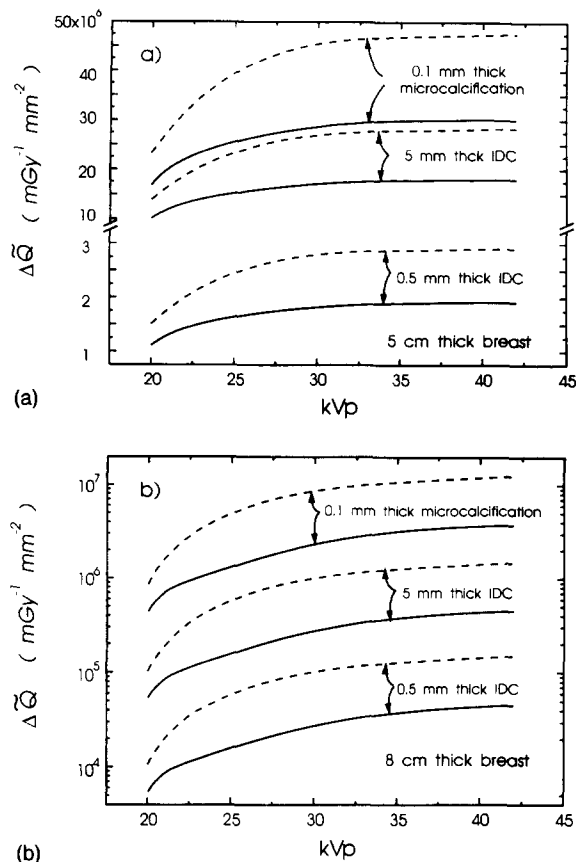
FIG. 9. The image signal per mm² per mGy mean glandular dose to the breast, $\Delta\tilde{Q}$, is shown for three lesions: the 0.5 mm thick IDC; the 5 mm thick IDC; and the 0.1 mm thick microcalcification. The data for Mo (solid) and W (dashed) spectra of varying kVp are shown in (a) for the 5 cm thick 50/50 breast, and in (b) for the 8 cm thick fibroglandular breast.
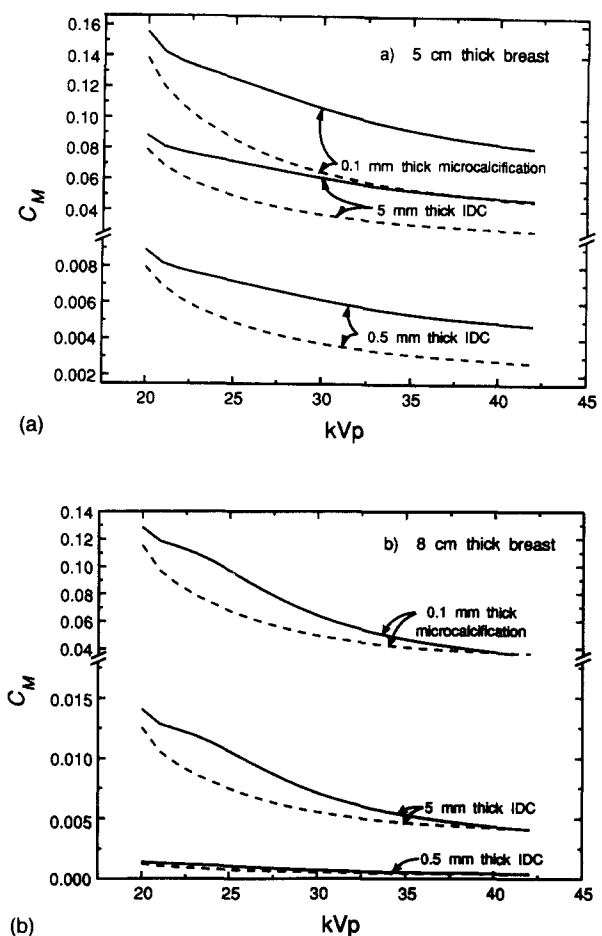
FIG. 10. The modulation contrast of the three lesions imbedded in (a) the 5 cm thick 50/50 breast and in (b) the 8 cm thick fibroglandular breast, for Mo (solid) and W (dashed) spectra.

of the fact that Mo spectra produce carrier signals that are smaller than those produced by W spectra, the Mo spectra produce greater modulation contrast. The difference is nearly a factor of 2. It is for this reason that Mo spectra are used in film-screen mammography, where subject contrast is the main goal.

In digital mammography, acquisition and display processes are separate; hence display contrast can be enhanced after acquisition by performing simple digital image enhancement such as "windowing and leveling." Therefore, if the x-ray carrier signals were noiseless, W spectra would be preferable in digital mammography because greater difference signals are produced, while producing a smaller value of Γ_C. However, in the presence of noise, LSNR must also be considered. In Figs. 11(a) and 11(b), the LSNR normalized by $k=5$ and by $D_g^{1/2}$ is shown for the three lesions in the 5 and 8 cm thick breasts, respectively. The optimal combination of target material and applied tube potential is that which produces the greatest value of the LSNR.[23] For lesions in the 5 cm thick breast, Mo and W spectra do not produce significantly different values of LSNR. Hence the increase in LSNR that is obtained with the Mo spectra may not be adequate to justify the increase in the required number of gray levels, since this may require a detector

with a higher value of Γ_D than is currently available. In the 8 cm breast, W spectra produce higher values of normalized LSNR than Mo spectra, while at the same time requiring fewer gray levels to display the same structure. For these reasons, W spectra are preferable for the use in digital mammography.

B. Real detector

In a more realistic digital mammography detector, losses occur between the phosphor screen and the image array (i.e., $C_D < 1$), and inherent detector noise is unavoidable (i.e., $\sigma_D > 0$). Again, we will assume that an ideal grid is used. In Fig. 12, the effect of C_D and σ_D on DQE is shown, while in Fig. 13, the effect on Γ_S (and equivalently, the effect on LSNR) is shown. The values of DQE, Γ_S, and hence LSNR are presented as a fraction of their values, DQE_{ideal}, $\Gamma_{S\ ideal}$, and $LSNR_{ideal}$, obtained with the idealized detector. In Fig. 14, the minimum required dynamic range (Γ_D) and minimum acceptable value of Q_{sat} are shown. The data are calculated for σ_D values of 0, 10, 10^2, 10^3, and 10^4 electrons per pixel, and are plotted as a function of $\bar{g}C_D$, the number of secondary quanta (in electrons) in the carrier signal per x-ray quantum interacting in the phosphor.
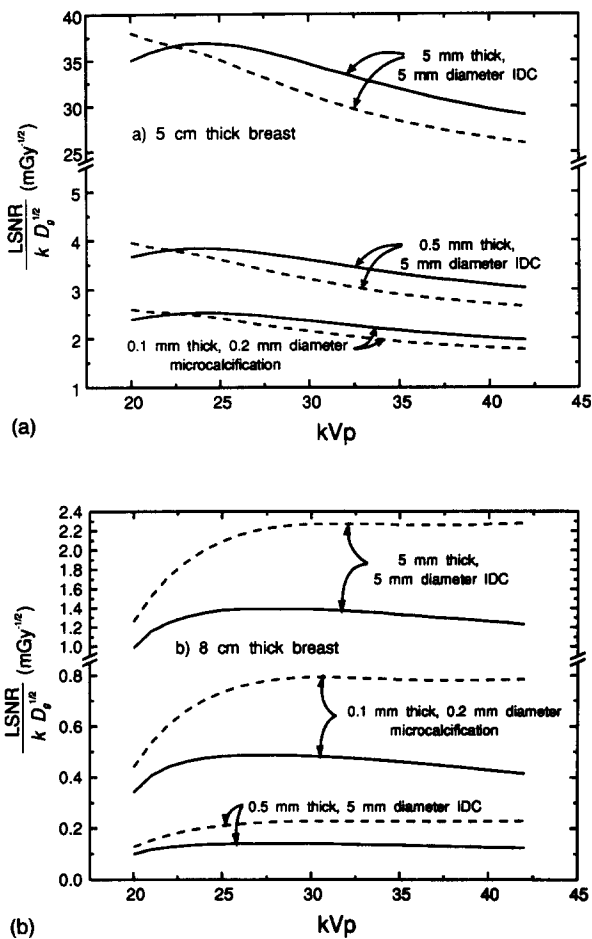
(a)

(b)

FIG. 11. $\mathrm{LSNR}/(kD_g^{1/2})$, assuming $k=5$, as defined by Rose's criterion, calculated for the three lesions shown. The data are calculated for Mo spectra (solid) and W spectra (dashed), for (a) the 5 cm thick and (b) the 8 cm thick breasts.
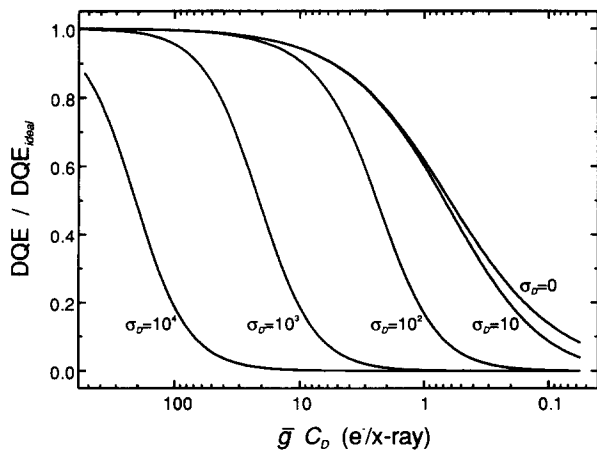

FIG. 12. The factor by which DQE is reduced due to coupling efficiency $(\bar{g}C_D)$ and inherent detector noise (σ_D). The factor was calculated for a 40 kVp W x-ray source, with a mean glandular dose to the 5 cm thick breast of 0.6 mGy. The inherent detector noise is specified in electrons per pixel.
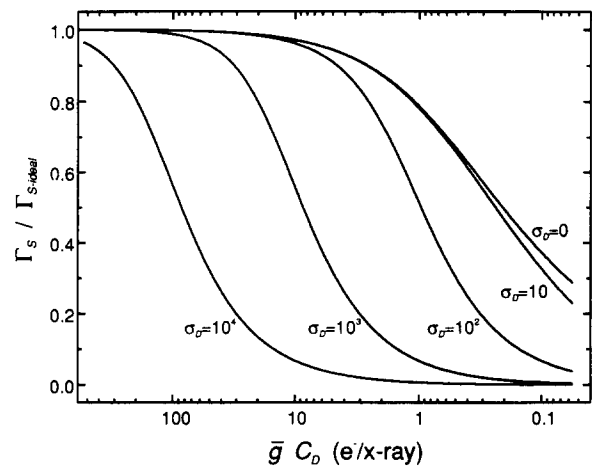

FIG. 13. The factor by which Γ_S (and equivalently, LSNR) is reduced due to coupling efficiency $(\bar{g}C_D)$ and inherent detector noise (σ_D). The factor was calculated for a 40 kVp W x-ray source, with a mean glandular dose to the 5 cm thick breast of 0.6 mGy.

The data shown in Figs. 12–14 were calculated for $a_P=0.05\times0.05$ mm^2, a 40 kVp W spectrum, and a mean glandular dose of 0.6 mGy to the 5 cm thick breast. With this spectrum incident, the average value of $\eta=0.49$ and $\bar{g}=470$. After filtration by the breast, the average values are $\eta=0.38$; $A_S=0.56$; and $\bar{g}=540$. In the shadow of the breast, $N_B=1440$ x rays interact with the phosphor per pixel on average, and in the air region, $N_A=1.37\times10^4$ x rays per pixel; hence $\Gamma_C=9.5$. With ideal coupling, the maximum carrier signal is 6.4×10^6 electrons.

First, the effect of varying the total coupling efficiency, $\bar{g}C_D$, will be considered for $\sigma_D=0$. Reducing the coupling efficiency causes DQE, Γ_S, and LSNR to decrease. This is due to an increase in the ratio of secondary quantum noise to x-ray quantum noise. At $\bar{g}C_D=1$, the DQE has been reduced by a factor of approximately $(1+A_S)^{-1}$ (a decrease of about 38%), and Γ_S and the LSNR have been reduced by a factor of approximately $(1+A_S)^{-1/2}$ (a de-
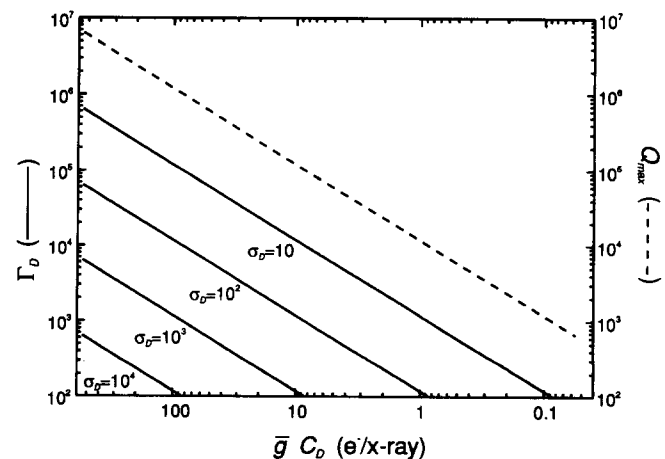

FIG. 14. The dynamic range (solid) and required minimum saturation carrier signal (dashed) of the Min-R medium screen based detector with varying coupling efficiency and inherent detector noise.
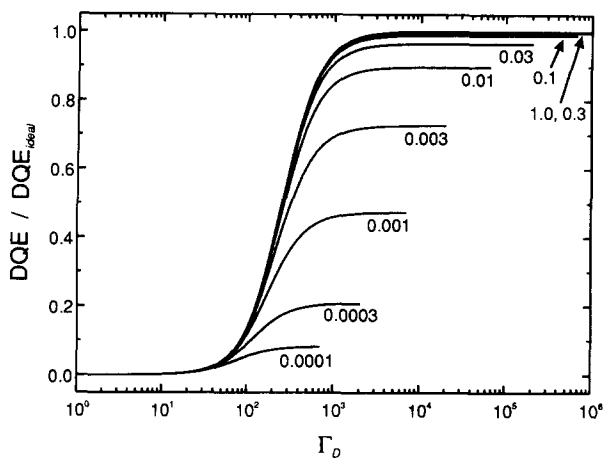
FIG. 15. The factor by which DQE is reduced due to coupling efficiency (C_D) and detector dynamic range (Γ_D) [i.e., varying inherent detector noise (σ_D).] The factor was calculated for a 40 kVp W x-ray source, with a mean glandular dose to the 5 cm thick breast of 0.6 mGy. Values of C_D are inset.

FIG. 16. The factor by which Γ_S (and equivalently, LSNR) is reduced due to coupling efficiency (C_D) and detector dynamic range (Γ_D) [i.e., varying inherent detector noise (σ_D)]. The factor was calculated for a 40 kVp W x-ray source, with a mean glandular dose to the 5 cm thick breast of 0.6 mGy. Values of C_D are inset.
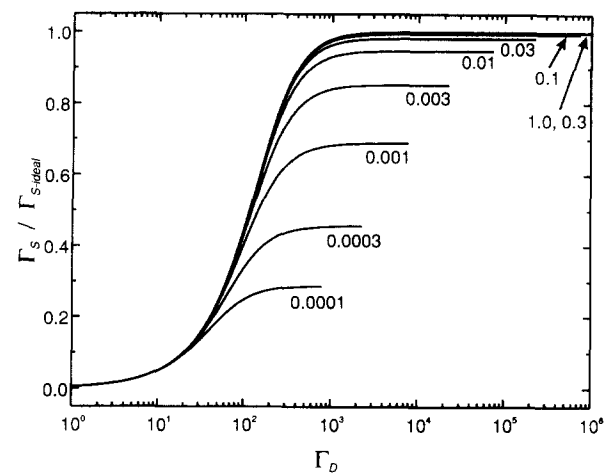
crease of about 21%). These approximations are valid when $\bar{g} \gg 1$. For values of $\bar{g}C_D \gg 1$, DQE, Γ_S, and LSNR are mainly dependent upon x-ray quantum noise, and, as such, do not vary greatly with $\bar{g}C_D$. For values of $\bar{g}C_D \approx 1$, the varying contributions of x-ray quantum and secondary quantum noise lead to rapid variation in the values of DQE, Γ_S, and LSNR. For $\bar{g}C_D \ll 1$, the images are dominated by secondary quantum noise, and hence the values of DQE, Γ_S, and LSNR approach zero. While the dynamic range (Γ_D) is undefined for $\sigma_D=0$, it is clear that the required value of Γ_D decreases linearly with decreasing coupling efficiency for a given value of σ_D. This occurs because the maximum detector signal, Q_{max}, is linearly related to the coupling efficiency.

Second, the effect of varying the inherent detector noise, σ_D, is considered. Clearly, increasing σ_D decreases DQE, Γ_S, and LSNR. The inherent detector noise is added in quadrature to the x-ray and secondary quantum noise. With increasing σ_D, DQE will be reduced by a factor of $(1+\sigma_D^2/\sigma_Q^2)^{-1}$, while Γ_S and LSNR will be reduced by a factor of $(1+\sigma_D^2/\sigma_Q^2)^{-1/2}$, where, in this instance, σ_Q^2 is calculated for $\sigma_D^2=0$. Therefore, in the presence of detector noise, increased coupling efficiency is required to ensure that x-ray quantum-noise-limited images are obtained.

In Figs. 15 and 16, DQE/DQE$_{ideal}$ and $\Gamma_S/\Gamma_{S\ ideal}$ are plotted versus dynamic range and coupling efficiency. Note that for $C_D=0.1$, a 5% reduction from $\Gamma_{S\ ideal}$ (and hence LSNR$_{ideal}$) occurs when $\Gamma_D=600$, and a 2% reduction occurs when $\Gamma_D=1000$. For the same value of C_D, a 5% reduction from DQE$_{ideal}$ occurs when $\Gamma_D=1200$, while a 2% reduction occurs when $\Gamma_D=2600$. If $C_D=0.03$, the effect of the inherent detector noise is more significant, and a 2% reduction from LSNR$_{ideal}$ occurs with $\Gamma_D=3000$. DQE, Γ_S, and LSNR decrease monotonically as coupling efficiency decreases and inherent detector noise increases. Since both coupling efficiency and inherent detector noise reduce the ratio of the x-ray quantum noise to the total

noise, the combination of coupling efficiency and inherent detector noise that produces the maximum LSNR should be used. Current CCD image arrays, with values of Γ_D between 10^3 and 10^4 and Q_{sat} values of between 10^5 and 10^6 electrons per pixel,[41] are only just acceptable for use in a digital mammography detector. Therefore, the optical coupling should be designed to ensure that the carrier signals span the entire range of charge that can be recorded by the image array.

The use of the data shown in Figs. 12–16 is illustrated by the following example for a detector similar to that shown in Fig. 1. Consider a typical image array with $Q_{sat}=6\times10^5$ electrons and $\sigma_D=120$ electrons (i.e., $\Gamma_D=5000$), and pixels of size $a_I=0.025\times0.025$ mm^2. The detector is optically coupled with a 2:1 demagnifying fiber-optic taper, giving pixels of size $a_P=0.05\times0.05$ mm^2 at the phosphor screen. The fiber-optic taper has an optical transmission efficiency of 14%, and the quantum efficiency of the CCD weighted over the spectral emission of the phosphor[42] is 0.45 electrons per light quantum. Hence, C_D has a value of 0.063 electrons per light quantum emitted from the screen. A summary of the results obtained with this detector configuration are presented in Table II, assuming $D_g=0.6$ mGy, and using both W and Mo spectra at 25, 30, 35, and 40 kVp.

The saturation carrier signal is one consideration when choosing an appropriate CCD and designing the optical coupling. As described above, CCD image arrays typically have a saturation carrier signal of 10^5–10^6 electrons, which can be the limiting factor in detector designs. Using the optical coupling described, a CCD with a saturation carrier signal of 4×10^5–6×10^5 electrons is required, depending on the target material, filtration, and applied tube voltage. Molybdenum spectra require CCD's with 20%–30% greater Q_{sat} values than W spectra.

Also shown in Table II are the image signal ratio (Γ_S), the image signal per pixel (ΔQ), and the LSNR of the

TABLE II. System requirements and signals generated by sample lesions for a typical breast (5 cm thick with two 0.4 cm thick adipose skin layers and a 4.2 cm thick 50% adipose, 50% fibroglandular core). The values of Q_{sat} and ΔQ are specified in electrons per pixel. The values of Γ_S were calculated for $a_L=0.0025$ mm^2 and $D_g=0.6$ mGy.

kVp	Q_{sat}	Γ_S	ΔQ 0.5 mm thick IDC	LSNR 0.5 mm thick IDC	ΔQ 5.0 mm thick IDS	LSNR 5.0 mm thick IDC	ΔQ 0.1 mm thick microcalc.	LSNR 0.1 mm thick microcalc.
Mo anode spectrum with 30 μm Mo filtration								
25	5.99×10^5	128.1	154	14.5	1430	135	2400	9.1
30	5.68×10^5	102.7	171	13.7	1610	129	2690	8.6
35	5.47×10^5	87.7	178	12.7	1680	119	2810	8.0
40	5.33×10^5	79.1	180	11.8	1700	112	2830	7.4
W anode spectrum with 1.0 mm Al filtration								
25	5.06×10^5	68.4	230	13.8	2190	131	3710	8.8
30	4.59×10^5	48.4	263	12.3	2530	118	4280	8.0
35	4.27×10^5	39.6	271	11.1	2620	107	4400	7.3
40	4.03×10^5	34.6	273	10.4	2650	101	4460	6.8

three lesions. Note that more gray levels are required to display the same structures when lower tube voltages and/or Mo spectra are used. The values of Γ_S were calculated assuming $a_L=a_P$ (i.e., for lesions occupying only a single pixel). The choice of maximum lesion size is related to the maximum aperture for which a human observer acts as an ideal observer. To perform this calculation for a given aperture size, it is necessary to multiply the value of Γ_S given in Table II by the square root of the number of pixels in the aperture [given by $(a_L/a_P)^{1/2}$]. For example, with the 40 kVp W spectrum and a circular aperture of diameter 5.0 mm (covering approximately 7800 pixels), $\Gamma_S=3100$.

X-ray quantum fluctuations should be visible on a pixel-to-pixel basis. To detect these fluctuations in the carrier signal, a fine quantization is required. If, for example, four gray levels per standard deviation are provided (i.e., $k'=20$), about 700 gray levels would be required to observe quantum fluctuations, assuming pixel-to-pixel carrier signal variations are independent. For an ideal observer to observe quantum fluctuations integrated over a large area, more gray levels would be necessary. For example, to record quantum fluctuations between regions 5 mm in diameter with $k'=20$ would require 6×10^4 gray levels. This is beyond the capabilities of modern image detectors, and is unnecessary. Instead, it is reasonable to assume that a digitization factor of $k'=1$ is sufficiently fine to ensure visualization of this lesion by an ideal observer. Therefore, only 3100 gray levels should be recorded. Hence with 12-bit digitization, both the minimum image signal and the pixel-to-pixel x-ray quantum fluctuations would be visible.

C. No grid

When, in addition to the primary radiation, scattered radiation is detected, the carrier signals (Q_A, Q_B, and Q_L) and the noise (σ_A, σ_B, and σ_L) increase for a given dose to the breast. As a result, the carrier signal ratio (Γ_C) and the number of discernable gray levels (Γ_S) will decrease compared to the nonscatter case. For mammographic energies, the scatter-to-primary ratio (SPR) does not change significantly with applied tube potential,[9,43] therefore, it has been assumed that the SPR is a constant. Dance et al.[9] have

calculated the SPR as a function of position for a 5 cm breast (50% fat, 50% fibroglandular composition–28 kVp Mo spectrum with 30 μm Mo filtration). They found the scatter fluence near the edge of the breast is approximately half that found at the center. Using these data, it is calculated that the SPR is $I''_B/I'_B=0.64$ in the breast and lesion regions and is 0.5 I''_B/I'_A in the region immediately surrounding the breast. It is estimated that $I''_B/I'_B=1.09$ for the 8 cm breast. These data are in agreement with measured SPR values.[8]

The fact that many of the scattered x-ray quanta will strike the detector obliquely increases the probability of interaction with the phosphor. Therefore, Q''_B/Q'_B will be greater than I''_B/I'_B. The ratio of x-ray interaction efficiencies, $\eta''(E)/\eta'(E)$, increases with increasing energy, hence Q''_B/Q'_B is greater for spectra with higher mean x-ray energy and for breasts that are more attenuating. For example, at 30 kVp with the 5 cm thick adipose and fibroglandular breast, $Q''_B/Q'_B=0.69$ for the Mo spectra and 0.74 for the W spectra, while with the 8 cm thick fibroglandular breast $Q''_B/Q'_B=1.26$ and 1.32, respectively. Outside the breast, the value of Q''_A is less than 3% of Q'_A for the 5 cm thick breast, and less than 0.5% for the 8 cm thick breast. The net effect is that Γ_C decreases with the detection of scatter. At 30 kVp, this decrease is 40% for the 5 cm thick breast and 56% for the 8 cm thick breast.

Since both Q_B and Q_L increase with the addition of scatter, the fluctuation in the image signal, $\sigma_{\Delta Q}$, increases. At 30 kVp, the effect causes $\sigma_{\Delta Q}$ to increase by 30% for the 5 cm thick breast, and by 52% for the 8 cm thick breast. Because of the increase in noise, Γ_S decreases by 23% with the 5 cm thick breast, and by 34% with the 8 cm thick breast. Hence, the detectability of subtle lesions is degraded and the number of gray levels that may be resolved decreases.

In previous results,[23] we showed that the addition of an antiscatter grid reduces the LSNR per unit mean glandular dose to the breast. That calculation was performed for a 5 cm thick, 50% adipose, 50% fibroglandular breast with W spectra, 100 μm rhodium filtration, and applied voltages between 20 and 42 kVp. The reduction in LSNR occurred

because the decrease in the image signal, brought about by the removal of primary radiation by the grid, is greater than the decrease in noise provided by the removal of scattered radiation. As a result, the use of a grid is not recommended in digital mammography systems using area detectors with linear energy response.

A scanned-slot detector behaves almost like an ideal grid with nearly 100% transmission of primary radiation and 5% scatter transmission for a 3 mm slot. Area detectors, therefore, will not be able to resolve as many gray levels as scanned-slot detectors that exhibit dose-efficient scatter reduction. However, use of a scanned-slot detector will increase image acquisition time and x-ray tube loading.

V. CONCLUSIONS

In a digital mammographic system, detectability of a lesion is primarily determined by the lesion signal-to-noise ratio. We have found that a W anode x-ray source provides equal LSNR to a Mo source for a 5 cm breast and superior LSNR for an 8 cm breast. This is in spite of the superior contrast and DQE (of the carrier signal) with Mo. Furthermore, the maximum carrier signal requirement for a system based on a W source is lower, as is the dynamic range required of the detector. Since the saturation carrier signal of CCDs is generally a limiting factor, a W source facilitates design of a digital mammographic system.

In considering the dynamic range requirements of digital mammography systems, we have shown that a detector with $C_D=0.03$ and $\Gamma_D=3000$ will reduce LSNR and the number of discernable gray levels by only 2%, compared to a detector with perfect coupling and no inherent detector noise, if a 40 kVp W spectrum is used. Molybdenum spectra require detectors with a dynamic range twice that required with a W spectrum.

With the 40 kVp W spectrum, 3100 gray levels are discernable ($k'=1$, $a_L=19.6$ mm^2). This requires that 12 bits of data be recorded per pixel.

When scattered radiation is present in the image, Q_{max} increases and Γ_S is reduced due to increased noise. In an example with a 30 kVp Mo spectrum and a 5 cm thick breast, scattered radiation resulted in a 30% increase in $\sigma_{\Delta Q}$, a 3% increase in Q_{max}, and a 23% reduction in Γ_S. Hence, area detectors without grids can resolve fewer gray levels than scanning-slot detectors that exhibit dose efficient scatter reduction.

The predictions in this paper are amenable to testing on a prototype system by measurements involving contrast-detail phantoms in which phantom thickness, lesion area, and lesion contrast can be altered.

ACKNOWLEDGMENTS

[a] Current address: Department of Radiology, Thomas Jefferson University, 3390 Gibbon Building, 111 South 11th Street, Philadelphia, PA, 19107-5098.

[1] D. B. Kopans, "Nonmammographic breast imaging techniques: Current status and future developments," Rad. Clin. North Am. 25, 961–971 (1987).

[2] D. B. Kopans, J. E. Meyer, and N. Sadowsky, "Breast Imaging," New England J. Med. 130, 960–967 (1984).

[3] E. A. Sickles, "Breast imaging: A view from the present to the future," Diagn. Imag. Clin. Med. 54, 118–125 (1985).

[4] R. M. Nishikawa, G. E. Mawdsley, A. Fenster, and M. J. Yaffe, "Scanned projection digital mammography," Med. Phys. 17, 717–727 (1987).

[5] J. M. Sabol and D. B. Plewes, "Latitude limitations of film-screen mammography," Med. Phys. 18, 1076 (1991).

[6] P. C. Bunch, K. E. Huff, and R. Van Metter, "Sources of noise in high-resolution screen-film radiography," Proc. SPIE 626, 64–75 (1986).

[7] R. M. Nishikawa and M. J. Yaffe, "Signal-to-noise properties of mammographic film-screen systems," Med. Phys. 12, 32–39 (1985).

[8] G. T. Barnes and I. A. Brezovich, "The intensity of scattered radiation in mammography," Radiology 126, 243–247 (1978).

[9] D. R. Dance, J. Persliden, and G. A. Carlsson, "Calculation of dose and contrast for two mammographic grids," Phys. Med. Biol. 37, 235–248 (1992).

[10] A. D. A. Maidment and M. J. Yaffe, "Scanned-slot digital mammography," Proc. SPIE 1231, 316–326 (1990).

[11] A. D. A. Maidment, B. G. Starkoski, G. M. Mawdsley, I. C. Soutar, N. R. Bennett, D. B. Plewes, and M. J. Yaffe, "A clinical scanned-slot digital mammography prototype," Med. Phys. 19, 1139 (1992).

[12] A. D. A. Maidment, M. J. Yaffe, D. B. Plewes, G. E. Mawdsley, I. C. Soutar, and B. G. Starkoski, "Imaging performance of a prototype scanned-slot digital mammography system," Proc. SPIE 1896, 93–103 (1993).

[13] A. Rose, *Vision: Human and Electronic* (Plenum, New York, 1973), pp. 21–23.

[14] R. E. Sturm and R. H. Morgan, "Screen intensification systems and their limitations," Am. J. Roentgenol. Radium Ther. 62, 617–634 (1949).

[15] J. W. Motz and M. Danos, "Image information content and patient exposure," Med. Phys. 5, 8–22 (1978).

[16] E. L. Dereniak and D. G. Crowe, *Optical Radiation Detectors* (Wiley, New York, 1984), pp. 250–251.

[17] H. P. Chan and K. Doi, "Monte Carlo simulation in diagnostic radiology," in *Monte Carlo Simulation in the Radiological Sciences*, edited by R. L. Morin (CRC Press, Boca Raton, 1988), p. 156.

[18] D. R. Dance and G. J. Day, "Simulation of mammography by Monte Carlo calculation—The dependence of radiation dose, scatter and noise on photon energy," in *Proceedings of Patient Exposure to Radiation in Medical X-ray Diagnosis*, edited by G. Drexler, H. Eriskat, and H. Schiobilla, EUR 7438, Brussels, Commission of the European Communities, 1981, pp. 227–243.

[19] D. R. Dance and G. J. Day, "The computation of scatter in mammography by Monte Carlo Methods," Phys. Med. Biol. 29, 237–247 (1984).

[20] M. J. Yaffe and R. M. Nishikawa, "X-ray imaging concepts: Noise, SNR, and DQE," in *Specification, Acceptance Testing, and Quality Control of Diagnostic X-ray Imaging Equipment*, edited by J. A. Siebert, G. T. Barnes, and R. G. Gould, AAPM Summer School, Santa Cruz, CA (in press).

[21] R. K. Swank, "Absorption and noise in x-ray phosphors," J. Appl. Phys. 44, 4199–4203 (1973).

[22] (a) D. M. Tucker, G. T. Barnes, and X. Wu, "Molybdenum target x-ray spectra: A semiempirical model," Med. Phys. 18, 402–407 (1991); (b) T. R. Fewell and R. J. Jennings (private communication, 1991).

[23] R. Fahrig, A. D. A. Maidment, and M. J. Yaffe, "Optimization of peak kilovoltage and spectral shape for digital mammography," Proc. SPIE 1651, 74–83 (1992).

[24] H. E. Johns and J. R. Cunningham, *The Physics of Radiology*, 4th ed. (Thomas, Springfield, IL, 1983), pp. 282–283.

[25](a) X. Wu, G. T. Barnes, and D. M. Tucker, "Spectral dependence of glandular tissue dose in screen-film mammography," Radiology **179**, 143–148 (1991); (b) X. Wu, G. T. Barnes, and D. M. Tucker (private communication, 1992).

[26]M. Rosenstein, L. W. Anderson, and G. G. Warner, *Handbook of Glandular Tissue Doses in Mammography*, FDA Publication 85–8239, Rockville, MD, 1985.

[27]L. N. Rothenberg, S. A. Feig, A. G. Haus, R. G. Jans, W. W. Logan, R. E. Shore, E. A. Sickles, and L. Stanton, *Mammography—A User's Guide*, NCRP Report 85 (National Council on Radiation Protection and Measurement, Bethesda, MD, 1987), pp. 40–41.

[28]E. A. Sickles, "Mammographic features of 300 consecutive nonpalpable breast cancers," Am. J. Roentgen. **146**, 661–663 (1986).

[29]H. S. Gallagher and J. E. Martins, "An orientation to the concept of minimal breast cancer," Cancer **28**, 1505–1507 (1971).

[30]R. R. Millis, R. Davis, and A. J. Stacey, "The detection and significance of calcifications in the breast: A radiological and pathological study," Brit. J. Rad. **49**, 12–26 (1976).

[31]K. A. Tonge, R. Davis, and R. R. Millis, "The problem of discrimination in mammography. Arguments for using a biological test object," Brit. J. Rad. **46**, 678–685 (1976).

[32]E. A. Sickles, "Mammographic detectability of breast microcalcifications," Am. J. Roentgen. **139**, 913–918 (1982).

[33]E. A. Sickles, "Breast calcifications: Mammographic evaluation," Radiology **160**, 289–293 (1986).

[34]E. F. Plechaty, D. E. Cullen, and R. J. Howerton, *Tables and Graphs of Photon Interaction Cross Sections from 1.0 keV to 100 MeV Derived from the LLL Evaluated Nuclear Data Library* (Lawrence Livermore Laboratory, Livermore, CA, 1975).

[35]P. C. Johns and M. J. Yaffe, "X-ray characterization of normal and neoplastic breast tissue," Phys. Med. Biol. **32**, 675–695 (1987).

[36]I. Othman, N. M. Spyrou, J. L. Price, and N. M. Gibbs, "Ultrastructure and composition of breast calcification using electron microscopy and microprobe analysis," in *Euroanalysis III*, edited by D. M. Carroll (Applied Science Publishers Ltd., London, 1979).

[37]R. Birch, M. Marshall, and G. M. Ardran, *Catalogue of Spectral Data for Diagnostic X-rays*, HPA Scientific Report Series 30, Hospital Physicists' Association, 1979, p. 134.

[38]D. P. Trauernicht and R. Van Metter, "Conversion noise measurement for front and back x-ray intensifying screens," Proc. SPIE **1231**, 262–270 (1990).

[39]C. E. Dick and J. W. Motz, "Utilization of monoenergetic x-ray beams to examine the properties of radiographic intensifying screens," IEEE Trans. Nucl. Sci. **NS-28**, 1554–1558 (1981).

[40]G. T. Barnes and D. P. Chakraborty, "Radiographic mottle and patient exposure in mammography," Radiology **145**, 815–821 (1982).

[41]E. L. Dereniak and D. G. Crowe, *Optical Radiation Detectors* (Wiley, New York, 1984), Chap. 9.

[42]E. H. Eberhardt, "Source–detector spectral matching factors," Appl. Opt. **7**, 2037–2047 (1968).

[43]G. A. Carlsson, D. R. Dance, and J. Persliden, "Grids in mammography: Optimization of the information content relative to radiation risk," Department of Radiation Physics, University of Linköping, Report No. ULi-RAD-R-059, 1989.